Topographic Wetness Index as a proxy for soil moisture: the importance of flow-routing algorithm and grid resolution

Henri Riihimäki[*, 1], Julia Kemppinen[*, †, 2], Martin Kopecký[3, 4] & Miska Luoto[1]

[1] *Department of Geosciences and Geography, University of Helsinki, Helsinki, Finland*

[2] *Geography Research Unit, University of Oulu, Oulu, Finland*

[3] *Institute of Botany of the Czech Academy of Sciences, Průhonice, Czech Republic*

[4] *Faculty of Forestry and Wood Sciences, Czech University of Life Sciences Prague, Prague, Czech Republic*

* Shared first authorship

† Corresponding author: Julia Kemppinen, julia.kemppinen@oulu.fi

Abstract

The Topographic Wetness Index (TWI) is a commonly used proxy for soil moisture. The predictive capability of TWI is influenced by the flow-routing algorithm and the resolution of the Digital Elevation Model (DEM) that TWI is derived from. Here, we examine the predictive capability of TWI using 11 flow-routing algorithms at DEM resolutions 1 - 30 m. We analyze the relationship between TWI and field-quantified soil moisture using statistical modelling methods and 5200 study plots with over 46 000 soil moisture measurements. In addition, we test the sensitivity of the flow-routing algorithms against vertical height errors in DEM at different resolutions. The results reveal that the overall predictive capability of TWI was modest. The highest R^2 (23.7%) was reached using a multiple-flow-direction algorithm at 2 m resolution. In addition, the test of sensitivity against height errors revealed that the multiple-flow-direction algorithms were also more robust against DEM errors than single-flow-direction algorithms. The results provide field-evidence indicating that at its best TWI is a modest proxy for soil moisture and its predictive capability is influenced by the flow-routing algorithm and DEM resolution. Thus, we encourage careful evaluation of algorithms and resolutions when using TWI as a proxy for soil moisture.

1 Introduction

Globally, the availability of high-resolution topographic data has increased due to recent developments in remote sensing technologies, such as light detection and ranging (LiDAR). At the same time, a wide selection of algorithms has become available through free and open-source software. A commonly used application of open algorithms and topographic data is the Topographic Wetness Index (TWI), which is a proxy for soil moisture (Beven & Kirkby, 1979; Seibert et al., 2007; Wilson 2018; Mattivi et al., 2019; Kopeckÿ et al, 2021). Consequently, it is important to evaluate how well this proxy relates to field-quantified soil moisture, and how the predictive capability of TWI changes depending on a given algorithm and data, such as the Digital Elevation Model (DEM), on which TWI is based on. Previously, the focus has been on either the algorithm (e.g., Sørensen et al., 2006; Kopecký & Čížková, 2010; Kopecký et al., 2021) or DEM resolution (e.g. Zhang & Montgomery, 1994; Gillin et al., 2015). However, rarely both algorithm and resolution are considered simultaneously.

TWI was developed for hydrological modelling (Beven & Kirkby, 1979; Wilson 2018). TWI can be used to locate saturated areas that create run-off and to estimate average groundwater levels (Rinderer et al., 2014). In addition to hydrological applications, TWI is widely used as a proxy for soil moisture, for instance, in vegetation science (Naito and Cairns, 2011; Raduła et al., 2018), geomorphology (Luoto & Hjort, 2005; Aalto et al., 2014), microclimate research (Ashcroft et al., 2008; Greiser et al., 2018; Macek et al., 2019), and carbon stock research (Pei et al., 2010; Mishra & Riley, 2012; Obu et al., 2017). Despite its common use, relatively few studies have investigated how well TWI relates to field-quantified soil moisture (see for instance, Sørensen et al., 2006; Buchanan et al., 2014; Raduła et al., 2018; Kopecký et al., 2021), chiefly due to the scarcity of spatially extensive soil moisture measurements (Sørensen & Seibert, 2007).

TWI consists of two parts; contributing catchment area per unit contour length (m^2/m) called the specific catchment area (SCA) and the local slope in radians (tan β) (Equation 1).

$$TWI = ln\left(\frac{SCA}{tan\beta}\right) (1),$$

SCA accounts for accumulated water, whereas the local slope accounts for the local gravitational force moving the accumulated water downwards (Quinn et al., 1991). Equation 1 assumes that soil transmissivity is constant throughout the catchment area. In the original TOPMODEL framework, transmissivity is used to control the effect of hydraulic gradient described by tanβ (Equation 1). Several algorithms exist for calculating both the local slope and SCA (Gruber & Peckham, 2009). Many studies use different algorithms for calculating TWI, however, they lack detailed descriptions on what algorithm they used (Kopecký & Čížková, 2010). This unfortunately decreases the overall reproducibility and comparability of results among studies (Kopecký et al., 2021).

The spatial resolution and accuracy of the original elevation data also influence TWI (Zhou and Liu, 2002). Inaccurate elevation data may lead to erroneous flow-routing (SCA) and slope values. In addition, DEM resolution determines how fine-scale landforms are represented in DEM, and consequently, in TWI. DEM resolution should be high enough to represent features, which are vital for the response (Quinn et al., 1995; Dark & Bram, 2007). For example, the fine-scale spatial variation of soil moisture is influenced by local landforms, such as small ridges and depressions (Thomas et al., 2017). However, if the response is chiefly influenced by coarse-scale landforms, higher resolution DEM does not automatically result in an improved outcome (Quinn et al., 1991; Sørensen & Seibert, 2007; Gillin et al., 2015). For example, groundwater distribution operates on a coarser scale than soil moisture and, thus, it is more related to the catchment area at a 3 - 5 m resolution rather than at a 1 m resolution (Gillin et al., 2015; Sørensen & Seibert, 2007). All in all, if the response varies at a fine-scale and DEM resolution does not match that scale, important information can be lost (Beven, 1998).

DEM resolution directly affects TWI (Quinn et al., 1995; Sørensen & Seibert, 2007; Vaze et al., 2010). The slope values (tan β) of a low-resolution DEM have a narrower distribution in comparison to a high-resolution DEM. This is caused by the loss of topographic detail, that is, averaging of the steepest slopes. Furthermore, flow paths are generally shorter with low-resolution data and less routing takes place. In general, larger TWI values are achieved using low-resolution DEMs (Quinn et al., 1995; Gillin et al., 2015). Most of the fundamental flow-routing algorithms have been published decades ago, therefore, they are based on medium-resolution DEMs (10 m or coarser). However, the recent developments in 3D remote sensing have allowed more realistic and accurate modelling of topography in comparison to the traditional medium-resolution DEMs. For example, LiDAR, high resolution RADAR, and Structure-from-Motion can provide extremely detailed information on topography. High-resolution data capture very fine-scale landforms (Barber & Shortridge, 2005; Jones et al., 2008; Vaze et al., 2010; Hasan et al., 2012; Thomas et al., 2017). A higher sampling rate offers more control over DEM resolution, as the high-resolution point clouds can be gridded to a proper resolution, which tackles some of the key issues in DEM resolution (Quinn et al., 1995).

Several studies have raised the concern of the impact of DEM resolution on TWI (Hancock, 2005; Wolock & Price, 1994; Zhang & Montgomery, 1994). Especially high-resolution DEMs have gained attention as more DEMs are openly available (Gillin et al., 2015; Hasan et al, 2012; Sørensen & Seibert, 2007; Thomas et al., 2017). However, it is still insufficiently known how DEM resolution and accuracy influence different flow-routing algorithms. Moreover, little is known about the performance of TWI as a proxy for soil moisture (Buchanan et al., 2013; Schröter et al., 2015; Radula et al., 2018; Qiu et al., 2017). Here, we 1) quantify the predictive capability of TWI as a proxy for soil moisture, 2) compare 11 flow-routing algorithms at different DEM resolutions, and 3) test the sensitivity of the algorithms against vertical height errors in DEM at different resolutions.

2 Materials and methods

2.1. Data

2.1.1. Field data

We measured soil moisture from 5200 plots (Riihimäki, Kemppinen et al. 2021) located in the northwestern Fennoscandian tundra, on Mount Saana and Mount Jehkas in Kilpisjärvi, Finland (69°03´N, 20°51´E; 582 - 808 meters above sea level (asl)) (Figure 1). Topography in the area is heterogenous, as the landscape is an alternation of hilltops, ridges, depressions, and steep slopes. The surficial deposits in the area consist of peat, fluvial deposits, glacial till, boulders, and rock outcrops (Kemppinen et al., 2018). The soils are poorly developed (median 10 cm depth, average 13 cm depth) covered with an organic layer (median 4 cm depth, average 6 cm depth) (Kemppinen et al., 2018). The vegetation type in the area is chiefly dwarf shrub tundra (Kemppinen et al, 2021). The annual precipitation is 518 mm (1991–2018; Kyläkeskus meteorological station; 69.04 N, 20.80 E; 480 m asl) (Finnish Meteorological Institute 2019a). The mean annual temperature is -3.1°C (1991–2018; Saana meteorological station; 69.04 N, 20.85 E; 1002 m asl) (Finnish Meteorological Institute 2019b).

First, we located 6000 plots (1 m^2) hierarchically. Secondly, we situated 1200 center plots systematically at 50 m intervals within an area of 2000 m $\times$ 1500 m. Then at 5 m from each center plot, we situated four more plots at each cardinal direction. We refer to a center plot with the four cardinal plots as a site (n = 1200). In the analyses, we used data from 1040 sites (n = 5200 plots), as we excluded sites that lacked data (for instance, sites partially under snow). We performed the analyses at two scales: 1 m^2 and 100 m^2. In the first scale, we use volumetric water content (VWC) of the center plot (n = 1040). In the latter scale, we use the plots at the cardinal directions (n = 4160) to calculate the mean VWC of the four plots (n = 1040). The location of the center plots were located using a hand-held GNSS receiver, with an accuracy up to $\leq$ 6 cm under optimal circumstances (GeoExplorer GeoXH 6000 Series; Trimble Inc., Sunnyvale, CA, USA).

We measured soil moisture (VWC) at each plot using a hand-held time-domain reflectometry sensor (FieldScout TDR 300; Spectrum Technologies Inc., Plainfield, IL, USA). The accuracy of the instrument is 3.0% VWC% with electrical conductivity < 2 dS m-1. VWC was measured up to a depth of 7.5 cm. To account for possible spatial variation within a given plot, we repeated the measurements at three points within each plot and used the average of the three measurements. To account for possible temporal variation during the growing-season, we repeated the measurements on three occasions during the growing-season of 2016 (June, July, August) and used the average of the three measurements (see Kemppinen et al., 2018 for further details). Altogether, each plot represents the average of nine measurements, which means that in total, we use 46 800 soil moisture measurements (Riihimäki, Kemppinen et al. 2021).
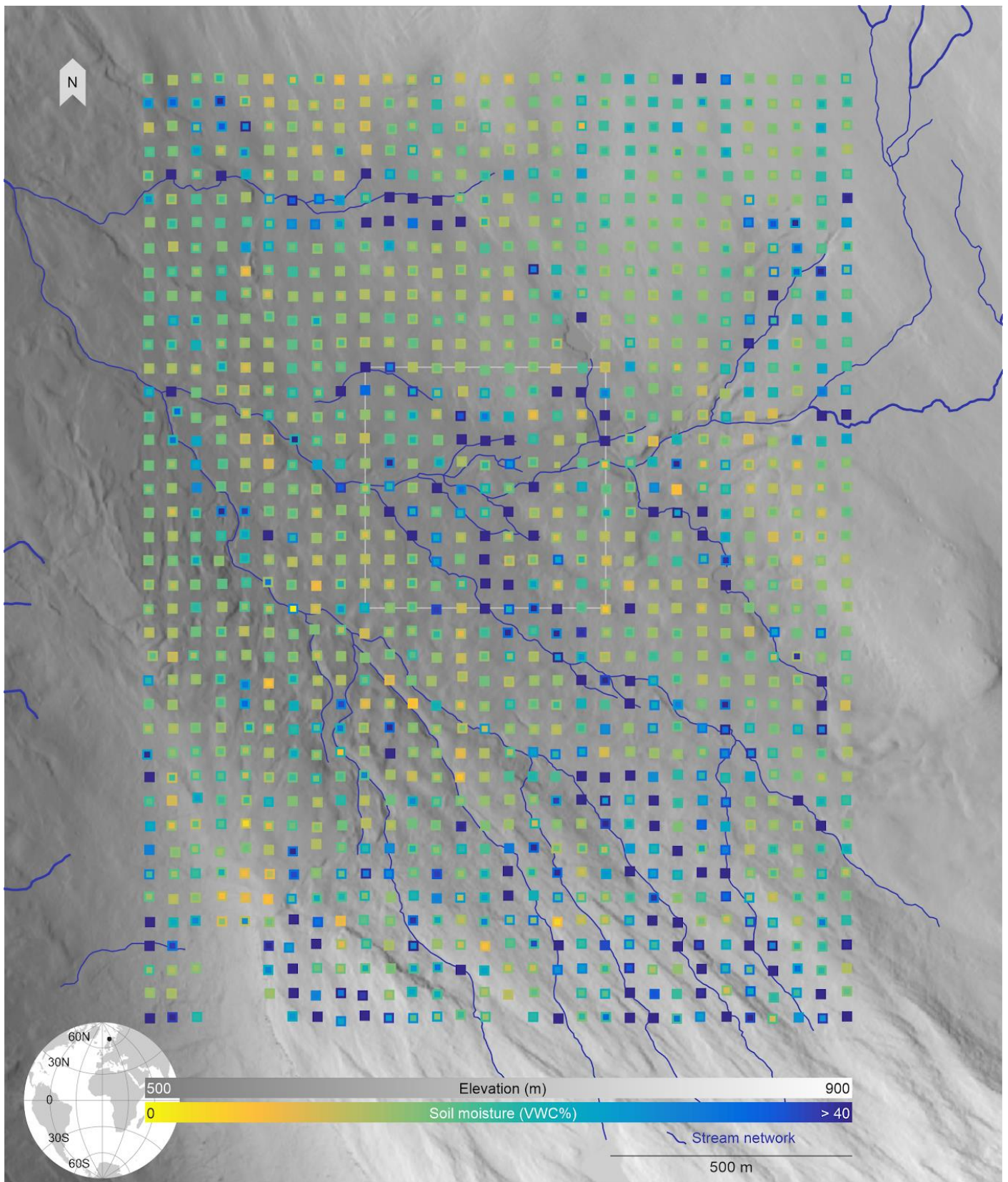
Figure 1. Field measurements of soil moisture. The squares represent the mean soil moisture, which is based on three independent measurements collected during the growing-season. Squares on top represent soil moisture measured at the 1 m²-scale, whereas the bottom squares represent the 100 m²-scale. This means that if the squares differ in color, there is fine-scale spatial variation in soil moisture. The white square represents the zoom-in area represented in Figure 2, 4, and 5. The elevation map with hillshade is based on a Digital Elevation Model provided by the National Land Survey of Finland, who also provided the stream network. Volumetric water content = VWC%.

2.1.2. LiDAR data

We used DEM data that was based on airborne laser scanning provided by the National Land Survey of Finland (2019). The study area was scanned with a Leica ALS60 laser scanner in August 2016 (leaf-on), with a pulse density of ~ 0.5 pulses/ m^2, and a nominal pulse spacing of ~ 1.4 m. The maximum scan angle was set to 20°, beam divergence to (1/e2) 0.22 mrad and flight altitude to cirka 2200 m above ground level. The accuracy of the z-coordinate is < 15 cm. The ground-classified point-cloud was converted to DEM by using the las2dem tool in LAStools software (version 170302) with an output resolution from 1, 2, ... 30 m (Isenburg, 2017). The tool first creates a triangulated TIN-model, which is then converted into grid format. For DEM resolution ≤ 2 m, we used all observations inside the pixel. For DEM resolution ≥ 3 m, we used a thinned point cloud by choosing the median point with a sample frequency set to resolution / 2 m (that is, Nyquist frequency). This step was done using the lasthin tool (Isenburg, 2017).

2.2. Methods

2.2.1. Topographic Wetness Index

We used SAGA GIS (v. 2.12) for calculating TWI. First, we used a filled DEM following the algorithm of Wang and Liu (2006) and calculated the local slope (Zevenbergen & Thorne, 1987). Then, we calculated the total catchment areas from the filled DEMs using the Catchment area-modules available in SAGA GIS (Table 1). Lastly, we calculated TWI for each of the 11 flow-routing algorithms and different DEM resolutions (1 - 30 m) using the TWI module.

Table 1. Flow-routing algorithms. n is the maximum number of cells, to which flow can be dispersed.

Algorithm	Abbreviation	*n*	Reference
Deterministic single-flow	D8	1	O'Callaghan & Mark, 1984
Stochastic single-flow	Rho8	1	Fairfield & Leymarie, 1991
Aspect driven kinematic routing	KRA	1	Lea, 1992
DEM networks	DEMON	2	Costa-Cabral & Burges, 1994
Braunschweiger relief model	BR	3	Bauer et al., 1985
Deterministic infinity	Dinf	2	Tarboton, 1997
Multiple-flow Dinf	MDinf	8	Seibert & McGlynn, 2007
Multiple-flow Freeman	FD8f	8	Freeman et al., 1991
Multiple-flow Quinn	FD8q	8	Quinn, 1991
Multiple-flow Holmgren	FD8h	8	Holmgren, 1994
Iteratively modified FD8f	SAGA algorithm	8	Böhner & Selige, 2006

We used flow-routing algorithms that chiefly followed the methodology and abbreviations in Kopecký and Čížková (2010) and Kopecký et al. (2021). We used 11 algorithms, which were available in the Hydrology-module of SAGA GIS (v. 2.12) (Conrad et al. 2015). We did not include more flow-routing algorithms, because these algorithms were either not yet available in any GIS software (Pilesjö & Hasan 2014; Orlandini

et al. 2003; Shelef & Hilley 2013) or were available only in commercial softwares, such as Mass Flux Method (Gruber & Peckham, 2009). We compare different single-flow-direction and multiple-flow-direction algorithms, which gives a good general understanding on how these commonly used algorithms affect the explanatory power of TWI. We give a brief description on the algorithms, but for a comprehensive review the algorithms we recommend reading Wilson (2018).

2.2.1.1. Specific catchment area

In SAGA GIS, the output of the most flow-routing algorithms is the total catchment area (TCA). However, the TWI formula requires the specific catchment area (SCA), which is calculated as TCA/L, where L is the flow-width per unit contour length. With gridded data, a common and effective solution is to assume that flow occurs through a pixel, thus, the flow-width is assumed to be identical to the resolution of the input data (Chirico et al., 2005). In SAGA GIS, this is referred to as pseudo-Specific Catchment Area (pSCA) (Conrad et al., 2015).

2.2.1.2. Creek initiation threshold area

In addition to SCA, other components of TWI are local slope (tan β) and creek initiation threshold area (CIT) (Quinn et al., 1995). CIT describes the point in which water-flow forms a distinguishable stream, and where normal assumptions of TWI do not hold (Quinn et al., 1995; Sørensen et al., 2006). After CIT criteria is met, the flow is routed downward as a "creek area" and flow dispersal of flow does not occur. Sørensen et al. (2006) tested various CIT values, but did not find an optimal value (cf. Quinn et al., 1995). Sørensen et al. (2006) concluded that the parameter is dependent on multiple factors, such as slope, soil type, and seasonality. Furthermore, CIT is influenced by DEM resolution (Sørensen and Seibert, 2007; Quinn et al., 1995). Finally, a CIT threshold that is too low might cause grid bias error when dispersal-flow still occurs after the given threshold. Quinn et al. (1995) suggest that it may be necessary to analyze optimal CIT for each individual catchment and resolution separately. As choosing a suboptimal CIT can produce undesired artefacts, we decided not to use CIT in our analysis.

2.2.1.3. Flow-routing algorithms

Deterministic single-flow (D8) algorithm is the simplest of the flow-routing approaches. This method is widely used, as it is available in many GIS software (Gruber & Peckham, 2009). In D8, all water-flow is assigned to one of the eight neighboring pixels based on the direction of the steepest descent (O'Callaghan and Mark, 1984). This approach has several shortcomings. First, divergent flow from a pixel is not considered. Secondly, D8 is prone to grid bias in flat areas or when it is based on low-quality DEMs (Tarboton, 1997). Thirdly, water-flow is treated as a one-dimensional feature, occurring only from one cell center to another (Costa-Cabral and Burges, 1994). All this makes D8 sensitive to possible errors in DEM. Consequently, vertical height errors in DEM may direct all the flow accumulation to a wrong pixel, and hence to all downward cells as well.

Stochastic single-flow (Rho8) algorithm is a stochastic extension of the D8 algorithm. It divides water-flow randomly to one of the eight neighboring cells by using slope-weighted probabilities (Fairfield & Leymarie, 1991). This reduces the grid bias, but this also results in a different outcome in every run, which can be problematic especially in small catchments (Gruber & Peckham, 2009). Furthermore, lateral flow-channels might merge and converge randomly, causing error to the total catchment area (Costa-Cabral & Burges, 1994).

Aspect driven kinematic routing (KRA) algorithm is an aspect-driven approach (Lea, 1992). KRA first fits a plane through the pixel center elevations. Next, it calculates aspect vectors in 1° increments, which are used

to route flow across the pixels. Finally, KRA calculates the contributing area as the number of flow-paths passing through the cell multiplied by the cell area (Wilson et al., 2008).

DEM networks (DEMON) is also an aspect-driven approach. The flow is generated uniformly over the cell area and directed downslope as a two dimensional 'tube', allowing water-flow to disperse between two pixels (Costa-Cabral & Burges, 1994). Thus, in DEMON, the flow does not originate from the pixel center.

Braunschweiger relief model (BR) allows water flow to three neighbouring pixels (Bauer et al., 1985). BR divides the outflow to a cell with orientation nearest to the aspect of the source cell, and its two neighboring cells (Kopecký and Čížková, 2010).

Deterministic infinity (Dinf) algorithm was introduced by Tarboton (1997) to tackle simultaneously the over-dispersion of multiple-flow-direction algorithms and the grid bias of the single-flow-direction algorithms. In Dinf, one flow direction is assigned from each cell based on planar triangular facets. Thus, the draining area can be divided between two neighboring cells. The proportions of these cells are dependent on flow-direction and how the direction-line cuts through the cells. A potential shortcoming of Dinf is that the outflow cannot occur in more than one direction, when in reality the given area can drain towards two (or more) different directions.

Multiple-flow Dinf (MDinf) algorithm was introduced by Seibert & McGlynn (2007). Similar to the single-flow-direction algorithm Dinf, flow is dispersed according to the triangular facets in MDinf. However, MDinf allows dispersal to all neighboring cells in certain cases. The flow-routing of MDinf is identical to Dinf in planar, convex, or concave landforms, but it responds differently in ridges and saddles (Seibert and McGlynn, 2007). In these cases, MDinf behaves as a multiple-flow-direction algorithm, and the dispersion can be similarly controlled with the v-value (Equation 2).

Multiple-flow Freeman (FD8f), multiple-flow Quinn (FD8q), and multiple-flow Holmgren (FD8h) are multiple-flow-direction algorithms, which are able to divide flow accumulation into all eight neighboring pixels. The draining fraction of a pixel (d) to a neighboring cell (NBi) is calculated as follows: (Equation 2)

$$d_{NBi} = \frac{tan\,(\beta_{NBi})^v \times L_{NBi}}{\sum_{j=1}^{8} tan\,(\beta_{NBj})^v \times L_{NBj}}\,(2),$$

where L is the draining contour length and v the exponent, which controls the amount of flow dispersion (Gruber & Peckham, 2009; Quinn et al., 1995). Different versions of the algorithm have been published by several authors, each with different v-values (FD8f in Freeman, 1991; FD8q in Quinn et al., 1991; FD8h in Holmgren, 1994). FD8q uses a v-value of 1 and FD8f a v-value of 1.1. Whereas for FD8h, Holmgren (1994) recommends using values between 4 and 6, here we used 4 in FD8h. A higher v-value results in a stronger flow towards a steeper slope, whereas a lower value leads to more dispersed flow (Quinn et al., 1995). The original FD8q algorithm also included a different L-value for flow routed to diagonal and cardinal cells, but the implementation in SAGA GIS uses the same L-value for all directions (Kopecký et al., 2021). The ability of these multiple-flow-direction algorithms to divide flow to all of its neighbors is useful in topographic positions, where water flows to different directions, for example in a saddle or ridge. However, multiple-flow-direction algorithms might cause flow over-dispersion, particularly with a low v-value (Costa-Cabral & Burges, 1994; Tarboton, 1997).

Iteratively modified FD8f (SAGA algorithm) is an algorithm specific to SAGA GIS. In SAGA algorithm, FD8f is used for the calculation of catchment area which is then iteratively modified (Equation 3.1) according to the flow accumulations in the surrounding cells (Böhner & Selige, 2006; Kopecký et al., 2021). SAGA algorithm produces a spatially smoothed TWI distribution, which may reduce the effect of DEM artefacts and errors that are known to deteriorate spatial representation of hydrological models, especially in flat areas (Böhner & Selige, 2006; Wise, 2007). SAGA algorithm uses an iterative modification for the SCA, which simulates flow suction from the pixels in the immediate neighborhood (Equation 3.1; Equation 3.2):

$$SCA_M = SCA_{max} \left(\frac{1}{t}\right)^{\beta exp(t^\beta)} \text{ for } SCA < SCA_{max} \left(\frac{1}{t}\right)^{\beta exp(t^\beta)} (3.1)$$

$$TWI(mod.) = ln\left(\frac{SCA_M}{tan\beta}\right) (3.2),$$

where t-parameter controls the suction effect (that is, the capillary attraction in the soil voids), β the slope angle [arcs], SCA, SCAM, and tan β (local slope). The downside of SAGA algorithm is that the user must define the t-parameter subjectively. We used SCA, local slope and default slope weighting set to 1. We calculated the modified catchment area with different t-parameters (t = 2, 4, 8,…,256) to test the effect of this parameter. The default t-parameter in SAGA GIS (v 2.12) is t = 10.

2.2.2. Sensitivity against vertical height errors in Digital Elevation Model

LiDAR data is prone to many errors. The LiDAR system itself may cause errors (such as ranging error or positioning error), but also mapping conditions (atmospheric conditions, wind) and object properties (roughness) can cause errors. Although, several error-sources can be countered by accurate calibration of the system and in the post-processing of the data, yet, some errors are still likely to remain (Wei & Bartels, 2012). Consequently, any remaining vertical height errors in the input data may significantly affect LiDAR based DEMs, and in turn, for instance flow-routing in TWI, as more flow-routing takes place at higher resolutions (Woodrow et al., 2016). For example, a one hectare area in a conventional DEM at 10 m resolution has 100 cells, but in a LiDAR DEM at 1 m resolution it has 10 000 cells. Therefore, proper flow-routing and the quality of the topographic data is increasingly important as the resolution of the data increases.

We test the sensitivity of the flow-routing algorithms against vertical height errors in DEM. First, we added vertical height errors to the original point cloud (Lindsay 2006). We created a normally distributed error-vector equal to the number of height observations, with a mean of 0 and a standard deviation of 10 cm, which represents a typical height height error for airborne LiDAR data (Naesset, 2015; Wei & Bartels, 2012). Then, we added the error-vector to the original point cloud and calculated TWI using the same workflow as with the original, unmodified point cloud data. Lastly, we calculated Pearson's correlation between 1) TWI based on the original DEM and 2) TWI based on the simulated DEM with vertical height errors. A high correlation indicates that the given flow-routing algorithm is not sensitive to height errors, whereas a low correlation indicates high sensitivity to height errors in DEM data.

2.2.3. Statistical analysis

We used a generalized additive model (GAM) to model soil moisture using TWI as an explanatory variable (Hastie & Tibshirani, 1987). The model used a Gaussian error family and a logarithmic link function, and a smoothing function with k = 3. The model was run through a 10-fold cross-validation, where the data were split randomly to ten different equally-sized parts. For each cross-validation fold, 10% of the data was left aside for evaluation and the remaining part (90%) was used as the training set. Here, we reported the results as the mean values of the 10 folds. To fit the GAM, we used the mgcv package in R (R Core Team 2017; Wood, 2018).

3 Results

3.1. TWI as a proxy for soil moisture

The overall predictive capability of TWI as a proxy for soil moisture varied from poor to moderate (Figure 2). The highest R^2 of the models was 23.7% (1 m²-scale) and 27.2% (100 m²-scale). The lowest R^2 was < 0.01 (both scales). Soil moisture at the two scales had a strong correlation (r = 0.90) and a paired t-test did not show a significant difference in soil moisture at the two scales (mean 0.017, p-value = 0.918). Therefore, here on we report detailed results for only the 1 m²-scale (for main results regarding the 100 m²-scale, see Supporting information for Figure S1).
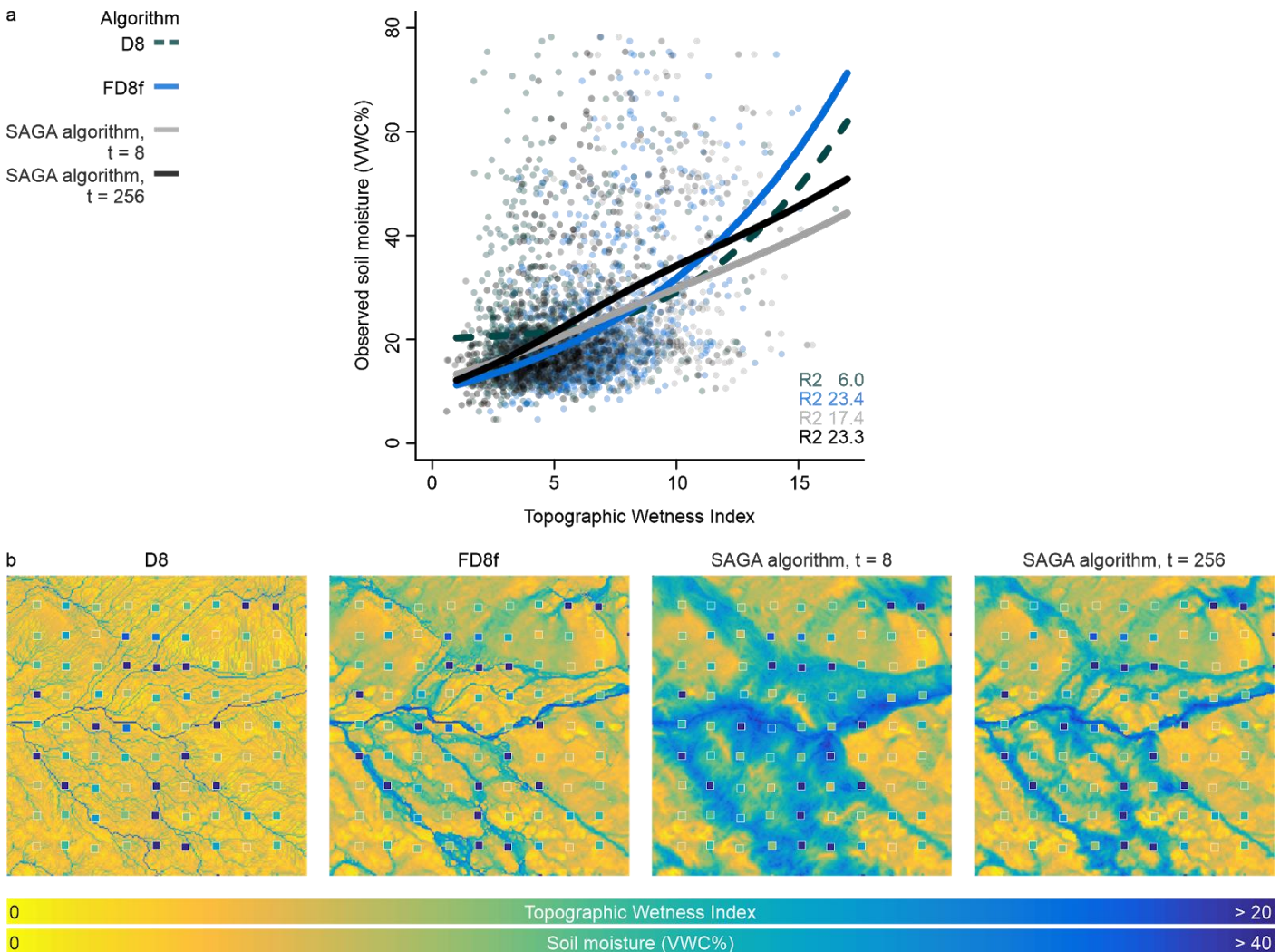
Figure 2. Topographic Wetness Index (TWI) as a proxy for soil moisture. Here, we present at 2 m resolution an example of a single-flow-direction algorithm (namely, D8) and a multiple-flow-direction algorithm (FD8f) as well as SAGA algorithm with two different t-parameters (that is, the suction effect). (a) The lines represent model fits of a generalized additive model. Dashed lines represent single-flow-direction algorithms and solid lines multiple-flow-direction algorithms. The points represent bivariate relationship between field measurements of soil moisture (1 m²-scale) and TWI values. (b) A zoom-in into the study area (white square in Figure 1) highlights the differences between algorithms. Squares represent soil moisture measured at the 1 m²-scale. This means that the greater the color difference between the squares and the underlying map, the greater the mismatch between soil moisture and the given TWI algorithm. Volumetric water content = VWC.

The maximal explanatory power was highest for soil moisture measured in June (FD8f at 2 m resolution, R^2 = 24.6%) and the lowest in August (FD8f at 2 m resolution, R^2 = 17.6%). However, the models regarding the

three time points (June, July, August) were similarly influenced by the flow-routing algorithms and resolutions. Therefore, here on we report detailed results for only the mean soil moisture level across the three time points (for main results for June, July, and August at the 1 m²-scale, see Figure S2, S3, and S4).

3.2. Comparing the flow-routing algorithms

The given flow-routing algorithm and resolution strongly influenced the explanatory power of TWI as a proxy for soil moisture (Figure 3a, 3b). Overall, none of the flow-routing algorithms reached their highest explanatory power at the 1 m resolution, which was the highest resolution in this comparison (Figure 3a). Overall, variation in the explanatory power increased at higher resolutions (Figure 3b).

D8 and Rho8 had low explanatory power at < 3 m resolutions (Figure 3a). D8 and Rho8 reached slightly better explanatory power at lower resolutions, but overall it remained low ($R2 < 0.13$).

KRA, DEMON, and BR reached similar explanatory power (Figure 3a). All three had low to no explanatory power at 1 - 2 m resolution. At 5 - 7 m resolution, they reached their maximum explanatory power, which decreased towards lower resolutions.

Dinf and MDinf reached similar explanatory power as the aspect-driven algorithms, namely KRA, DEMON, and BR (Figure 3a). Dinf reached its maximal explanatory power at 3 m resolution and MDinf had a slightly higher explanatory power at > 10 m resolution.

FD8f at 2 m resolution reached the highest explanatory power of all algorithms at all resolutions ($R2$ 23.7%) (Figure 3a). Overall, FD8f, FD8q, and FD8h showed very similar results and reached explanatory power of over 21%.

SAGA algorithm ($t = 256$) reached its highest explanatory power at ≤ 2 m resolution and its explanatory power decreased towards lower resolutions (Figure 3a). SAGA algorithm was tested with various t-parameters, that is, the suction effect. The highest t-parameter ($t = 256$) had the highest explanatory power of all t-parameters, and in general, higher t-parameters were associated with higher explanatory power (Figure 3c). At 1 m resolution, the explanatory power of SAGA algorithm ($t = 256$) exceeded FD8f by 5.6 percentage points (Figure 3a). Overall, variation in the explanatory power increased at higher resolutions (Figure 3d).

The main differences among the flow-routing algorithms and their performance at different resolutions are shown in Figure 4. For instance, D8, produced a structured stream network at 1 m resolution and had no explanatory power as a soil moisture proxy ($R2 = 0.01$). The explanatory power of D8 slightly increased at 10 m resolution. Whereas, FD8f, produced a smoother stream network due to its capability to disperse flow to multiple neighboring cells (eight cells). FD8f over-dispersed at lower resolutions (> 10 m), and this was even more obvious in SAGA algorithm, in which the neighboring area also affects the values a pixel is given. In SAGA algorithm, low t-parameter ($t = 8$) at low resolutions produced a smooth stream network and it had no explanatory power as a proxy for soil moisture.

3.3. Sensitivity against vertical height errors in DEM

In the test of sensitivity of the flow-routing algorithms against vertical height errors in DEM, the results indicated that TWI is sensitive to vertical height errors especially at high-resolutions (≤ 10 m) (Figure 5). Overall, the results were similar among all algorithms, but BR, FD8f, FD8q, and SAGA algorithm ($t = 256$) were the most robust algorithms against height errors. At > 5 m resolutions, the correlations between TWI values calculated from the original DEM and TWI values calculated from the simulated DEM with height errors were generally very high (> 0.9), except for D8 and Rho8, which performed relatively poorly. SAGA

10

algorithm was very robust against height errors (> 0.95) regardless of the given t-parameter, therefore, we report detailed results for only SAGA algorithm (t = 256).
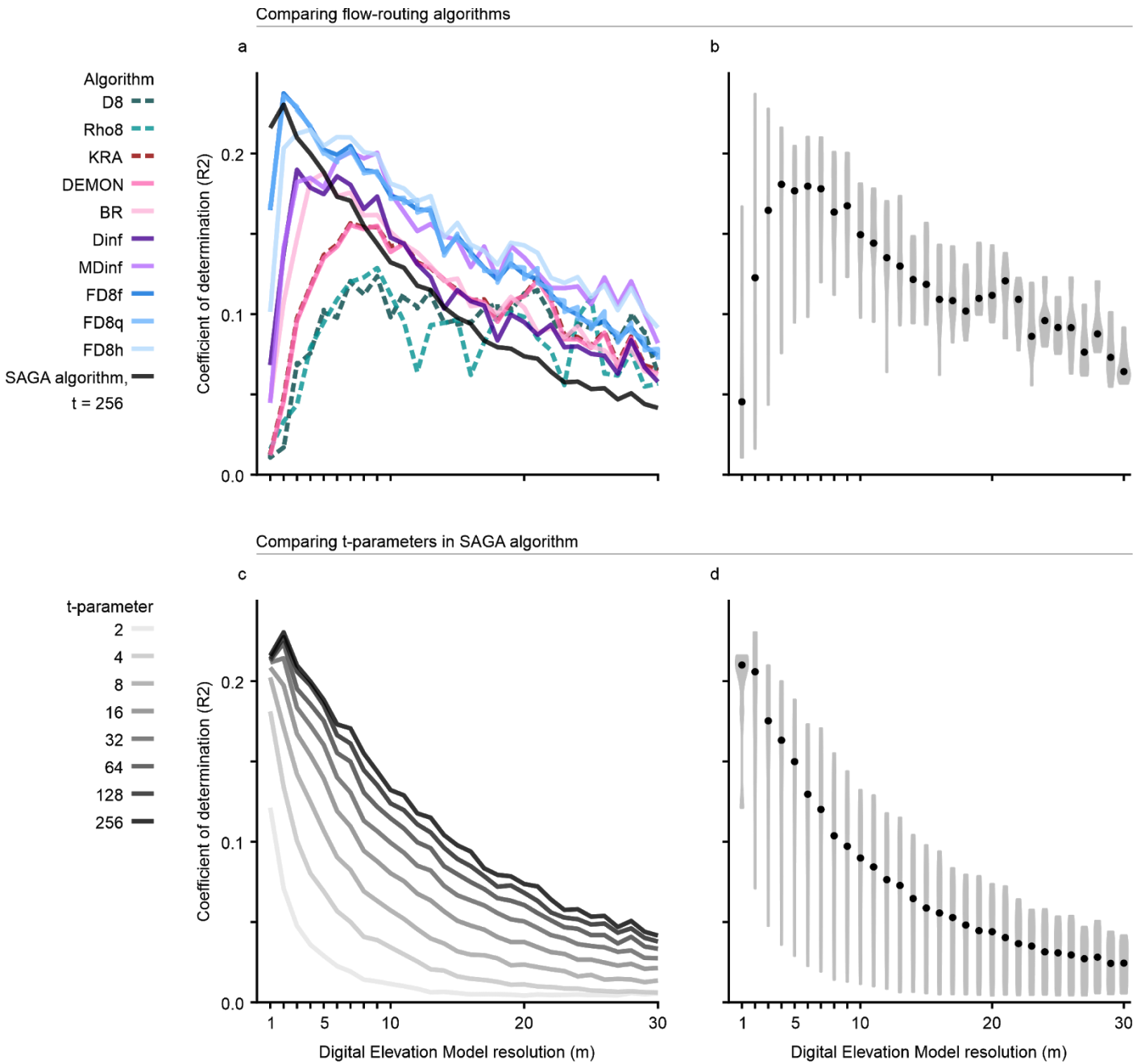
Figure 3. Comparing flow-routing algorithms and t-parameters (that is, the suction effect) with soil moisture measured at the 1 m²-scale. (a) Lines represent the explanatory power of the flow-routing algorithms at different Digital Elevation Model (DEM) resolutions. Dashed lines represent single-flow-direction algorithms and solid lines multiple-flow-direction algorithms. At 2 m resolution, FD8f reached the highest explanatory power and FD8q had only slightly lower explanatory power. (b) Violin plots represent the overall explanatory power of the flow-routing algorithms. (c) Lines represent the explanatory power of the t-parameters in SAGA algorithm at different DEM resolutions. At 2 m resolution, t-parameter 256 reached the highest explanatory power and 128 had only slightly lower explanatory power. (d) Violin plots represent the overall explanatory power of the t-parameters. In the violin plots (b, d), the thickness of the violin polygon corresponds to the local density of the values and the points represent the median values.

11
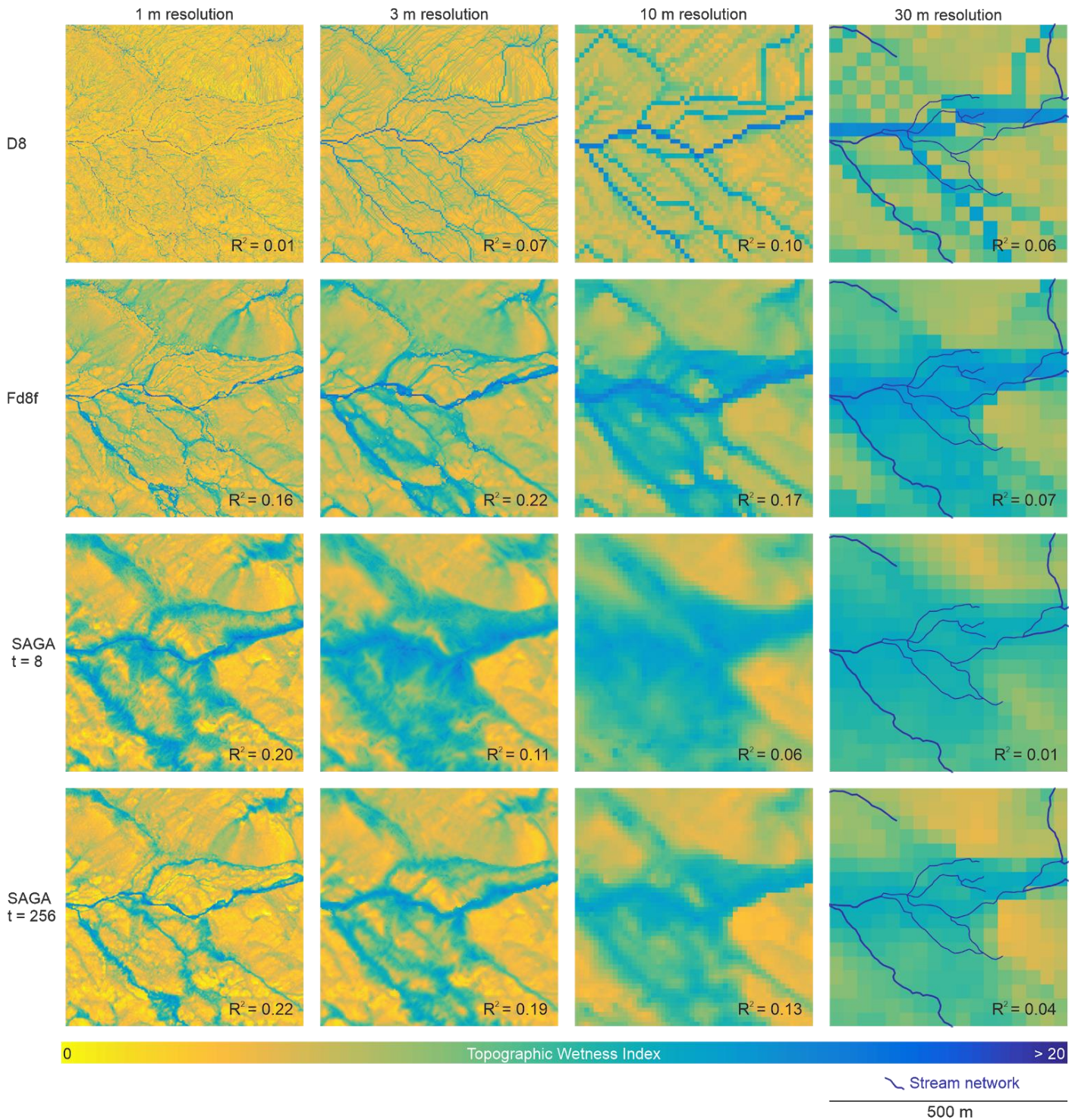
Figure 4. Flow-routing algorithms at different resolutions. Here, we present a single-flow-direction algorithm (namely, D8) and a multiple-flow-direction algorithm (FD8f) as well as SAGA algorithm with two different t-parameters (that is, the suction effect). A zoom-in into the study area (white square in Figure 1) highlights the differences between algorithms. For instance, at 1 m resolution, D8 produces a structured stream network, whereas FD8f a smoother stream network. At lower resolutions, FD8f over-disperses, which is further highlighted in SAGA. In SAGA, a small t-parameter (t = 8) and low resolution produces a smooth stream network. The stream network overlaid on the panels representing the 30 m resolution is provided by the National Land Survey of Finland.
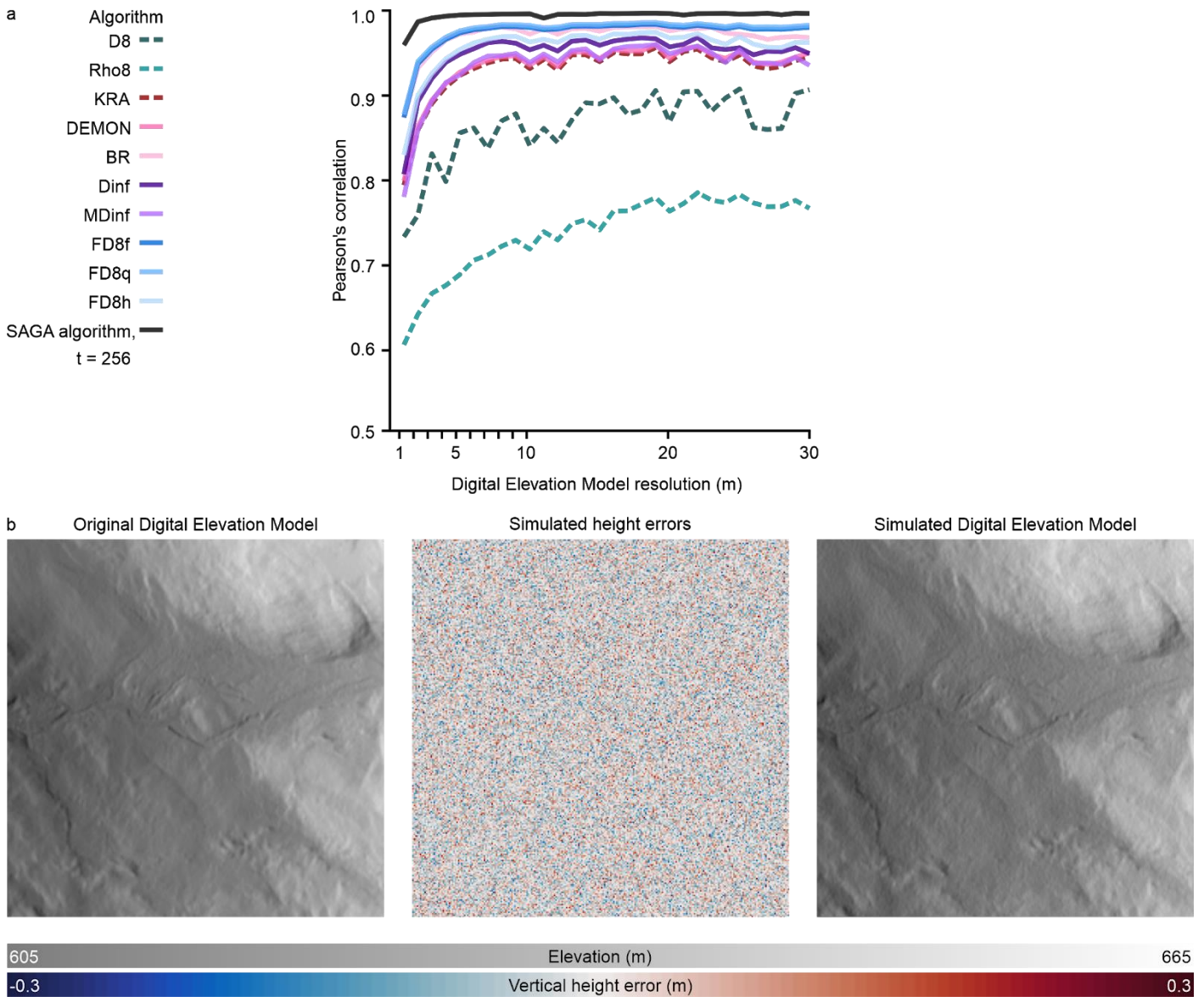
Figure 5. Sensitivity of the flow-routing algorithms against vertical height errors in Digital Elevation Model (DEM). (a) The lines represent Pearson's correlation between Topographic Wetness Index (TWI) values calculated from the original DEM and TWI values calculated from simulated DEM with vertical height errors. High correlation indicates that the algorithm is robust against height errors. Dashed lines represent single-flow-direction algorithms and solid lines multiple-flow-direction algorithms. Note that in the y-axis starts at 0.5. (b) A zoom-in into the study area (white square in Figure 1) represents the original DEM, simulated height errors, and the simulated DEM, that is the original DEM with simulated height errors.

4 Discussion

We quantified the predictive capability of TWI as a proxy for soil moisture using 5200 study plots. The results demonstrate that the explanatory power of TWI varied from very low to moderate (Figure 2), depending on the given flow-routing algorithm and DEM resolution (Figure 3). We compared 11 flow-routing algorithms at DEM resolutions 1 - 30 m. The results revealed that the highest explanatory power was reached using a multiple-flow-direction algorithm at high-resolution, namely FD8f at 2 m resolution (Figure 3a). However, the flow-routing algorithms reached their highest explanatory power at 4 - 7 m resolution (Figure 3b). In addition, we also tested the sensitivity of the algorithms against vertical height errors in DEM. The results indicate that TWI is sensitive to height errors and that multiple-flow-direction algorithms were more robust against height errors than single-flow-direction algorithms (Figure 5a). Overall, the results demonstrate that flow-routing algorithms do matter, especially at high-resolution, at which the flow-routing algorithms differ the most (Figure 4).

13

We recommend that researchers using TWI report in detail what flow-routing algorithm and DEM resolution they use for increasing reproducibility and comparability of their results. Our investigations provide motivation to explore also other proxies besides TWI, especially quantify their predictive capability for soil moisture and compare their algorithms at different resolutions. It would be interesting and very important to investigate for instance the downslope gradient (Hjerdt et al., 2004) and other topography-based alternatives to TWI, such as the Depth to Water index (Murphy et al., 2009) and the Height Above the Nearest Drainage index (Nobre et al., 2011), and also reflectance-based alternatives, such as the Tasseled-cap Wetness Index (Crist and Cicone, 1984). In light of our results, it is likely that both algorithm and resolution influence also their predictive capability for soil moisture.

4.1. TWI as a proxy for soil moisture

At its best, the explanatory power of TWI as a proxy for soil moisture was moderate in the tundra with relatively thin soils. TWI is based solely on topographic information, which is only one factor affecting the fine-scale spatial variation of soil moisture. Also other topography factors and soil and vegetation factors influence the spatial patterns of soil moisture (Quinn et al., 1995; Lookingbill & Urban, 2004; Kemppinen et al., 2021). Here, we used soil moisture data that Kemppinen et al. (2018) modelled with TWI (SAGA algorithm, t = 20, 1 m resolution) along with other DEM derived topography factors (namely, elevation, potential solar radiation, topographic position index) and field-quantified soil factors (surficial deposits, organic soil depth), which resulted in relatively high explanatory power (R^2 = 60%) (see Kemppinen et al., 2018). Nevertheless, TWI had the highest relative influence on the spatial patterns of soil moisture (Kemppinen et al., 2018), which supports the important influence that topography has on soil moisture. However, here our aim was not to build the best possible model for soil moisture, but rather examine how well this commonly used soil moisture proxy, namely TWI, explains field-quantified soil moisture and to understand how the flow-routing algorithm and DEM resolution influence the predictive capability of TWI.

Previous studies have reported that the hydrological response can vary within landscapes (Tague et al., 2010; Kaiser & McGlynn 2018). For instance, Seibert et al. (1997) suggested that the steady state assumption of TWI is not valid in all cases. Rinderer et al. (2014) examined if these assumptions are met in alpine catchments with shallow groundwater levels, which is similar to in our study area. TWI was found useful for predicting median groundwater level and the highest correlation between TWI and groundwater level was during the wettest time period (Rinderer et al., 2014). Instead of groundwater levels, here, we used TWI to examine soil moisture and found that the maximal explanatory power of TWI was highest in June, which is when the tundra landscape is relatively wet due to melting snow. Whereas, the explanatory power of TWI was lowest in August, which is when the landscape is relatively dry. However, our soil moisture data is based on three measurements (June, July, August), which do not describe all the full temporal variation of soil moisture throughout the growing-season (Kopecký et al., 2021). Thus, new devices for continuous soil moisture measurements could reveal even greater temporal variation in the explanatory power of TWI (Wild et al., 2019).

Overall, there is a demand for quantitative modelling of the fine-scale spatial variation of soil moisture, especially in vegetation science (Kopecký et al., 2021) and ecosystem studies (Liu et al. 2020). However, TWI can lead to erroneous conclusions on the role of soil moisture, if it is used as a direct proxy for soil moisture without considering the influence of flow-routing algorithms and DEM resolutions. For example, le Roux et al. (2013) used a single-flow-direction algorithm (D8, 1 m resolution DEM based on digital contour data) in modelling species' distributions and richness patterns and found that TWI decreased the explanatory power of the models. In contrast, field-quantified moisture data increased the explanatory power of the models, and revealed the importance of soil moisture for fine-scale vegetation patterns (le Roux et al., 2013). In another example, Riihimäki et al. (2017) used a multiple-flow-direction algorithm (SAGA algorithm, t = 10, 10 m resolution) in modelling above-ground biomass and productivity. However, here our results revealed that that

particular algorithm at that resolution has a low explanatory power for soil moisture. In turn, our results suggest that Riihimäki et al. (2017) possibly underestimated the importance of soil moisture for above-ground biomass and productivity. Nevertheless, it is unlikely that there is an universal flow-routing algorithm at a certain DEM resolution that best describes the role of soil moisture across ecosystems, due to the heterogeneity within and across ecosystems (Quinn et al., 1995; Sørensen et al. 2006). Nevertheless, these examples (le Roux et al., 2013; Riihimäki et al., 2017) stress 1) the importance of quantifying how well a given proxy relates to soil moisture and 2) the influence of flow-routing algorithms and DEM resolutions on the explanatory power of TWI.

4.2. Importance of flow-routing algorithms

The flow-routing algorithm controls how the accumulated water is calculated from DEM, and thus, directly affects the TWI values. In our analyses, we investigated different single-flow-direction algorithms, namely D8, Rho8, and KRA. The results revealed that these algorithmns had very low explanatory power at high-resolutions (< 5 m), where more flow-routing takes place. The test of sensitivity against vertical height errors in DEM also indicated that single-flow-direction algorithms are sensitive to possible height errors. Thus, their low explanatory power at high-resolutions is likely due to their sensitivity to height errors (Tarboton, 1997). Height errors in DEM affect single-flow-direction algorithms by increasing the risk of erroneous flow-routing, and consequently, errors in the catchment area estimate. For instance, Dinf had higher explanatory power than the single-flow-direction algorithms, which is probably due to the ability of Dinf to reduce grid bias by dividing flow accumulation area into two pixels (Tarboton, 1997). Another limitation of single-flow-direction algorithms is their inability of model divergent flow (Costa-Cabral & Burges, 1994). In addition, DEM resolution also influences the variation of the flow accumulation values and typically low-resolution data has lower variation than high-resolution data (Dark and Bram, 2007).

Overall, the multiple-flow-direction algorithms that we investigated had higher explanatory power than the single-flow-direction algorithms. Thus, our results from the tundra support previous findings from temperate forests (Kopecký et al., 2021). In agreement with these findings, our results revealed that especially FD8f and FD8q had high explanatory power. Multiple-flow-direction algorithms allow divergent outflow from a pixel, which can divide the outflow to multiple neighboring cells, which enables a more realistic flow. This is important, especially when a pixel contains water-flow dividing landform, such as a ridge or a hummock (Quinn et al., 1991; Erskine et al., 2006). The test of sensitivity against vertical height errors in DEM indicated that FD8f and FD8q were robust against height errors. Overall, multiple-flow-direction algorithms should be less sensitive against height errors than single-flow-direction algorithms, since water-flow can be dispersed between multiple neighbors in the multiple-flow-direction algorithms (Kopecký & Čížková, 2010). Thus, this is likely the reason why at high-resolutions, multiple-flow-direction algorithms have higher explanatory power than the single-flow-direction algorithms.

We also investigated SAGA algorithm, a modified version of the multiple-flow-direction algorithm FD8f. In SAGA algorithm, the catchment area is modified according to the maximum flow accumulation values in the pixel neighborhood, which should increase robustness against possible DEM errors (Böhner & Selige, 2006). This was indeed evident in the test of sensitivity against vertical height errors, in which SAGA algorithm (t = 256) was the most robust of all algorithms at all resolutions. Interestingly, the explanatory power of SAGA algorithm at 1 m resolution and FD8f at 3 m resolution were comparable. Thus, it would be more efficient to use FD8f at 3 m resolution, at least from a computational point of view. In addition, Kopecký et al. (2021) investigated TWI as a proxy for forest soil moisture and reported that the explanatory power of SAGA algorithm was less than half of FD8f. Furthermore, using SAGA algorithm at low-resolutions might cause over-dispersion, particularly when using a low t-parameter (that is, the suction effect) as is the default in SAGA GIS (t = 10). However, a low t-parameter produces extremely smooth patterns in TWI, which can be useful in e.g. modelling air temperature patterns affected by cold-air pooling (Macek et al. 2019).

Nevertheless, our results indicated that the default t-parameter (t = 10) in SAGA GIS is not optimal for calculation of TWI as a proxy for soil moisture in the tundra. Here, we found that the default t-parameter causes flow over-dispersion, which decreases the explanatory power of TWI.

4.3. Importance of DEM resolution

Higher DEM resolution does not necessarily result in an improved outcome in the explanatory power of TWI (Quinn et al., 1991; Sørensen & Seibert, 2007; Gillin et al., 2015). In our analyses, the highest explanatory power was not reached at the highest DEM resolution (1 m), that is, the scale of the soil moisture measured at the 1 m^2 study plots. In fact, the results indicated that the median explanatory power of all algorithms was at its lowest at 1 m resolution. Gillin et al. (2015) arrived at similar conclusions using TWI to model groundwater. In our study, it is possible that the fine-scale spatial variation of soil moisture is more influenced by general landforms controlling subsurface flow (that is, slopes, ridges, depressions) and less influenced by fine-scale topography controlling surface flow (small hummocks, large stones) (Sørensen & Seibert, 2007). Our results indicate a strong correlation between the two scales (1 m^2, 100 m^2), at which we measured soil moisture.

Low explanatory power at highest DEM resolution (1 m) can be due to the LiDAR data and its relatively low pulse density (~ 0.5 pulses/ m^2). Low sample rate in relation to DEM cell size can cause uncertainty in high-resolution DEMs (Hengl & Evans, 2009). In addition, the LiDAR point spacing (~1.4 m) was only slightly larger than the highest DEM resolution, which is not optimal. This is even more important to consider if DEM data contains vertical height errors, as this can affect the final products, such as TWI values (Wise, 2007; Lindsay & Evans, 2008; Hengl & Evans, 2009). In our test of sensitivity against vertical height errors in DEM, the results demonstrate that the flow-routing algorithms are the most sensitive at high-resolutions, but their sensitivity decreased towards lower resolutions. Nevertheless, the robustness against height errors varied among the flow-routing algorithms also at low-resolutions. Overall, high-quality DEMs (that is, higher sample density and accuracy) are needed to increase the explanatory power and noise-sensitivity of TWI (Hengl & Evans, 2009; Thomas et al., 2017).

5 Conclusions

Our results from the tundra indicated that TWI as a proxy for soil moisture had very low to moderate explanatory power. The explanatory power of TWI was depended on flow-routing algorithm and DEM resolution. Generally, multiple-flow-direction algorithms demonstrated higher explanatory power and more robustness against vertical height errors in DEM than single-flow-direction algorithms. Overall, our investigations provide field evidence on how well a commonly used proxy relates to soil moisture and highlights the importance of considering different algorithms and resolutions. In the case of TWI, the results emphasize that flow-routing algorithms do matter, especially at high-resolutions. We encourage researchers in search of a proxy for soil moisture 1) to carefully consider and report in detail what algorithm and resolution they use, 2) to evaluate the robustness of the algorithm against possible errors in DEM, and 3) to take into account that higher resolutions may not always be more suitable.

Data availability

The field data (Riihimäki, Kemppinen et al. 2021) is openly available in a data repository (Zenodo): https://doi.org/10.5281/zenodo.4590183 The laser scanning data produced by the National Land Survey of Finland is openly available: https://tiedostopalvelu.maanmittauslaitos.fi/tp/kartta?lang=en

Acknowledgments

Author contributions

HR conceptualised the research idea, processed and analysed the data and wrote the original draft. HR and JK performed the field investigations and visualised the data. JK, MK and ML reviewed and edited the original draft. HR, JK, MK and ML revised the manuscript based on peer review comments.

Permissions

Permission to carry out fieldwork was granted by Metsähallitus.

Competing Interests Statement

The authors have no competing interests.

References

Aalto, J., Venäläinen, A., Heikkinen, R. K. & Luoto, M. (2014). Potential for extreme loss in high-latitude Earth surface processes due to climate change. Geophysical Research Letters, 41, 3914-3924. https://doi.org/10.1002/2014gl060095

Ashcroft, M. B., Chisholm, L. A., & French, K. O. (2009). Climate change at the landscape scale: predicting fine-grained spatial heterogeneity in warming and potential refugia for vegetation. Global Change Biology, 15(3), 656-667. https://doi.org/10.1111/j.1365-2486.2008.01762.x

Barber, C. P. & Shortridge, A. (2005). Lidar Elevation Data for Surface Hydrologic Modeling: Resolution and Representation Issues. Cartography and Geographic Information Science, 32, 401-410. https://doi.org/10.1559/152304005775194692

Bauer, J., Rohdenburg, H. & Bork, H. R. (1985). Ein Digitales Reliefmodell als Vorraussetzung fuer ein deterministisches Modell der Wasser- und Stoff-Fluesse. In: Bork, H.R. & Rohdenburg, H. (eds.) Parameteraufbereitung fuer deterministische Gebiets-Wassermodelle, Grundlagenarbeiten zu Analyse von Agrar-Oekosystemen. pp. 1–15. Technische Universitat Braunschweig, Braunschweig, DE.

Beven, K. (1998). TOPMODEL: A critique. Hydrological Processes, 11, 1069-1085. https://doi.org/10.1002/(sici)1099-1085(199707)11:9<1069::aid-hyp545>3.3.co;2-f

Beven, K. J. & Kirkby, M. J. (1979). A physically based, variable contributing area model of basin hydrology / Un modèle à base physique de zone d'appel variable de l'hydrologie du bassin versant. Hydrological Sciences Bulletin, 24, 43-69, https://doi.org/10.1080/02626667909491834

Buchanan, B.P. Fleming M, Schneider RL, Richards BK, Archibald J, Qiu Z, et al. (2013). Evaluating topographic wetness indices across central New York agricultural landscapes. Hydrology and Earth System Sciences Discussions, 10(11), 14041–14093. http://dx.doi.org/10.5194/hessd-10-14041-2013

Böhner, J. & Selige, T. (2006). Spatial prediction of soil attributes using terrain analysis and climate regionalisation, in: Böhner, J., McCloy, K.R., Strobl, J. (Eds.), SAGA - Analyses and Modelling Applications. Verlag Erich Goltze GmbH, pp. 13-27.

Chirico, G. B., Western, A. W., Grayson, R. B. & Bloschl, G. (2005). On the definition of the flow width for calculating specific catchment area patterns from gridded elevation data. Hydrological Processes, 19, 2539-2556, https://doi.org/10.1002/hyp.5730

Conrad O., Bechtel, B., Bock, M., Dietrich, H., Fischer, E., Gerlitz, L., Wehberg, J., Wichmann, V. & Böhner J. (2015). System for Automated Geoscientific Analyses (SAGA) v. 2.1.4. Geoscientific Model Development, 8, 1991–2007.

Costa-Cabral, M. C. & Burges, S. J. (1994). Digital Elevation Model Networks (Demon) - a Model of Flow over Hillslopes for Computation of Contributing and Dispersal Areas. Water Resources Research, 30, 1681-1692. https://doi.org/10.1029/93wr03512

Crist, E. P. and Cicone, R. C. (1984) A Physically-Based Transformation of Thematic Mapper Data—The TM Tasseled Cap. IEEE Transactions on Geoscience and Remote Sensing, GE-22(3), 256–263. https://doi.org/10.1109/TGRS.1984.350619

Dark, S. J. & Bram, D. (2007). The modifiable areal unit problem (MAUP) in physical geography. Progress in Physical Geography, 31, 471-479. https://doi.org/10.1177/0309133307083294

Erskine R.H., Green T.R., Ramirez J. a. & MacDonald L.H. (2006) Comparison of grid-based algorithms for computing upslope contributing area. Water Resources Research 42: 1–9. https://doi.org/10.1029/2005WR004648

Fairfield, J. & Leymarie, P. (1991). Drainage Networks from Grid Digital Elevation Models. Water Resources Research, 27, 709-717. https://doi.org/10.1029/90wr02658

Finnish Meteorological Institute (2019a). Enontekiö Kilpisjärvi Kyläkeskus. Daily climate observations. https://en.ilmatieteenlaitos.fi/download-observations#

Finnish Meteorological Institute (2019b). Enontekiö Kilpisjärvi Saana. Daily climate observations. https://en.ilmatieteenlaitos.fi/download-observations#

Freeman, T. G. (1991). Calculating catchment area with divergent flow based on a regular grid. Computers & Geosciences, 17, 413–422. https://doi.org/10.1016/0098-3004(91)90048-i

Gillin, C. P., Bailey, S. W., McGuire, K. J. & Prisley, S. P. (2015). Evaluation of Lidar-derived DEMs through Terrain Analysis and Field Comparison. Photogrammetric Engineering and Remote Sensing, 81, 387-396. https://doi.org/10.14358/pers.81.5.387

Greiser, C., Meineri, E., Luoto, M., Ehrlen, J. & Hylander, K. (2018). Monthly microclimate models in a managed boreal forest landscape. Agricultural and Forest Meteorology, 250, 147-158. https://doi.org/10.1016/j.agrformet.2017.12.252

Gruber, S. & Peckham, S. (2009). Land-Surface Parameters and Objects in Hydrology. Geomorphometry: Concepts, Software, Applications, 33, 171-194. https://doi.org/10.1016/s0166-2481(08)00007-x

Hancock, G. R. (2005). The use of digital elevation models in the identification and characterization of catchments over different grid scales. Hydrological Processes, 19, 1727-1749, https://doi.org/10.1002/hyp.5632

Hastie, T. & Tibshirani, R. (1987). Generalized Additive-Models - Some Applications. Journal of the American Statistical Association, 82:371-386. https://doi.org/10.2307/2289439

Hasan, A., Pilesjö, P. & Persson A. (2012). On generating digital elevation models from lidar data – Resolution versus accuracy and topographic wetness index in Northern Peatlands. Geodesy and Cartography 38(2): 57-59. https://doi.org/10.3846/20296991.2012.702983

Hengl, T. & Evans, I.S. (2009). Mathematical and Digital Models of the Land Surface. Developments in Soil Science, 33, 31-63. https://doi.org/10.1016/S0166-2481(08)00002-0

Hjerdt, K.N., McDonnell, J.J., Seibert, J., Rodhe, A., 2004. A new topographic index to quantify downslope controls on local drainage. Water Resour. Res. 40, 1–6. https://doi.org/10.1029/2004WR003130

Holmgren, P. (1994). Multiple Flow Direction Algorithms for Runoff Modeling in Grid Based Elevation Models - an Empirical-Evaluation. Hydrological Processes, 8, 327-334. https://doi.org/10.1002/hyp.3360080405

Isenburg, M. (2017). LAStools - efficient LiDAR processing software (version 170302, Academic license).

Jones, K. L., Poole, G. C., O'Daniel, S. J., Mertes, L. A. K. & Stanford, J. A. (2008). Surface hydrology of low-relief landscapes: Assessing surface water flow impedance using LIDAR-derived digital elevation models. Remote Sensing of Environment, 112, 4148-4158. https://doi.org/10.1016/j.rse.2008.01.024

Kaiser K.E. & McGlynn B.L. (2018) Nested Scales of Spatial and Temporal Variability of Soil Water Content Across a Semiarid Montane Catchment. Water Resources Research 54: 7960–7980. https://doi.org/10.1029/2018WR022591

Kemppinen, J., Niittynen, P., Riihimäki, H. & Luoto, M. (2018). Modelling soil moisture in a high-latitude landscape using LiDAR and soil data. Earth Surface Processes and Landforms, 43, 1019-1031. https://doi.org/10.1002/esp.4301

Kemppinen, J., Niittynen, P., Virkkala, A.-M., Happonen, K., Riihimäki, H., Aalto, J. & Luoto, M. (2021). Dwarf Shrubs Impact Tundra Soils: Drier, Colder, and Less Organic Carbon. Ecosystems (2021). https://doi.org/10.1007/s10021-020-00589-2

Kopecký M. & Čížková, S. (2010). Using topographic wetness index in vegetation ecology: does the algorithm matter? Applied Vegetation Science, 13, 450-459. https://doi.org/10.1111/j.1654-109x.2010.01083.x

Kopecký, M., Macek, M. & Wild, J. (2021). Topographic Wetness Index calculation guidelines based on measured soil moisture and plant species composition. Science of The Total Environment, 757, 143785. https://doi.org/10.1016/j.scitotenv.2020.143785

Lea, N. L. (1992). An aspect driven kinematic routing algorithm, in: Parsons, A.J., Abrahams, A.D. (Eds.), Overland flow: Hydraulics and erosion mechanics. Chapman & Hall, New York, pp. 147-175.

Lindsay, J. B. (2006). Sensitivity of channel mapping techniques to uncertainty in digital elevation data. International Journal of Geographical Information Science, 20(6), 669–692. doi:10.1080/13658810600661433

Lindsay, J. B., & Evans, M. G. (2008). The influence of elevation error on the morphometrics of channel networks extracted from DEMs and the implications for hydrological modelling. Hydrological Processes, 1603(July 2007), 1588–1603. doi:10.1002/hyp.6728

Liu, L., Godmundsson, L., Hauser, M., Qin, D., Li, S., & Seneviratne, S. (2020). Soil moisture dominates dryness stress on ecosystem production globally. Nature Communications, 11, 4892. https://doi.org/10.1038/s41467-020-18631-1

Lookingbill, T. & Urban, D. (2004). An empirical approach towards improved spatial estimates of soil moisture for vegetation analysis. Landscape Ecology, 19, 417-433. https://doi.org/10.1023/b:land.0000030451.29571.8b

Luoto, M. & Hjort, J. (2005). Evaluation of current statistical approaches for predictive geomorphological mapping. Geomorphology, 67, 299-315. https://doi.org/10.1016/j.geomorph.2004.10.006

Macek, M., Kopecký, M., & Wild, J. (2019). Maximum air temperature controlled by landscape topography affects plant species composition in temperate forests. Landscape Ecology, 34(11), 2541–2556. doi:10.1007/s10980-019-00903-x

Mattivi P., Franci F., Lambertini A., & Bitelli G. (2019). TWI computation: a comparison of different open source GISs. Open Geospatial Data, Software and Standards 4, 6. doi:10.1186/s40965-019-0066-y.

Mishra, U. & Riley, W. J. (2012). Alaskan soil carbon stocks: spatial variability and dependence on environmental factors. Biogeosciences, 9, 3637-3645. https://doi.org/10.5194/bgd-9-5695-2012

Murphy, P. N. C., Ogilvie, J. and Arp, P. A. (2009). Topographic modelling of soil moisture conditions: A comparison and verification of two models. European Journal of Soil Science, 60: 94–109. https://doi.org/10.1111/j.1365-2389.2008.01094.x

Naesset, E. (2015). Vertical Height Errors in Digital Terrain Models Derived from Airborne Laser Scanner Data in a Boreal-Alpine Ecotone in Norway. Remote Sensing, 7, 4702-4725. https://doi.org/10.3390/rs70404702

National Land Survey of Finland (2019). Laser scanning data. https://www.maanmittauslaitos.fi/en/maps-and-spatial-data/expert-users/product-descriptions/laser-scanning-data (accessed 16.1.2019).

Naito, A. T. & Cairns, D. M. (2011). Relationships between Arctic shrub dynamics and topographically derived hydrologic characteristics. Environmental Research Letters, 6, 045506. https://doi.org/10.1088/1748-9326/6/4/045506

Nobre, A. D., Cuartas, L. A., Hodnett, M., Rennó, C. D., Rodrigues, G., Silveira, A., Waterloo, M., Saleska, S. (2011). Height Above the Nearest Drainage – a hydrologically relevant new terrain model. Journal of Hydrology, 404(1-2), 13–29. doi:10.1016/j.jhydrol.2011.03.051

O'Callaghan, J. F. & Mark, D. M. (1984). The Extraction of Drainage Networks from Digital Elevation Data. Computer Vision Graphics and Image Processing, 28, 323-344. https://doi.org/10.1016/s0734-189x(84)80047-x

Orlandini, S., Moretti, G., & Franchini, M. (2003). Path-based methods for the determination of nondispersive drainage directions in grid-based digital elevation models. Water Resources Research, 39(6), 1–8. doi:10.1029/2002WR001639

Obu, J., Lantuit, H., Myers-Smith, I., Heim, B., Wolter, J. & Fritz, M. (2017). Effect of Terrain Characteristics on Soil Organic Carbon and Total Nitrogen Stocks in Soils of Herschel Island, Western Canadian Arctic. Permafrost and Periglacial Processes, 28, 92-107. https://doi.org/10.1002/ppp.1881

Pei, T., Qin, C. Z., Zhu, A. X., Yang, L., Luo, M., Li, B. L. & Zhou, C. H. (2010). Mapping soil organic matter using the topographic wetness index: A comparative study based on different flow-direction algorithms and kriging methods. Ecological Indicators, 10, 610-619. https://doi.org/10.1016/j.ecolind.2009.10.005

Pilesjö P. & Hasan, A. (2014). A Triangular Form-based Multiple Flow Algorithm to Estimate Overland Flow Distribution and Accumulation on a Digital Elevation Model. Transactions in GIS 18(1): 108-124. https://doi.org/10.1111/tgis.12015

Qiu, Z., Pennock, A., Giri, S., Trnka, C., Du, X., & Wang, H. (2017). Assessing Soil Moisture Patterns Using a Soil Topographic Index in a Humid Region. Water Resources Management, 31(7), 2243–2255. doi:10.1007/s11269-017-1640-7

Quinn, P., Beven, K., Chevallier, P. & Planchon, O. (1991). The Prediction of Hillslope Flow Paths for Distributed Hydrological Modeling Using Digital Terrain Models. Hydrological Processes, 5, 59-79. https://doi.org/10.1002/hyp.3360050106

Quinn, P. F., Beven, K. J. & Lamb, R. (1995). The Ln(a/Tan-Beta) Index - How to Calculate It and How to Use It within the Topmodel Framework. Hydrological Processes, 9, 161-182. https://doi.org/10.1002/hyp.3360090204

R Core Team (2017). R: The R Project for Statistical Computing. In: R foundation for statistical computing, https://www.r-project.org/ (accessed 6th May 2018).

Raduła, M. W., Szymura, T. H. & Szymura, M. (2018). Topographic wetness index explains soil moisture better than bioindication with Ellenberg's indicator values. Ecological Indicators, 85, 172-179, https://doi.org/10.1016/j.ecolind.2017.10.011.

Riihimäki, H., Kemppinen, J., Kopecký, M. & Luoto, M. (2021). Data from: Topographic Wetness Index as a proxy for soil moisture: the importance of flow-routing algorithm and grid resolution. Zenodo. https://doi.org/10.5281/zenodo.4590183

Riihimäki, H., Heiskanen, J. & Luoto, M. (2017). The effect of topography on arctic-alpine aboveground biomass and NDVI patterns. International Journal of Applied Earth Observation and Geoinformation, 56, 44-53. https://doi.org/10.1016/j.jag.2016.11.005

Rinderer, M., van Meerveld, H. J., & Seibert, J. (2014). Topographic controls on shallow groundwater levels in a steep, prealpine catchment: When are the TWI assumptions valid? Water Resources Research, 50(7), 6067–6080. doi:10.1002/2013wr015009

le Roux, P. C., Aalto, J. & Luoto, M. (2013). Soil moisture's underestimated role in climate change impact modelling in low-energy systems. Global Change Biology, 19, 2965–2975. http://dx.doi.org/10.1111/gcb.12286

Schröter, I., Paasche, H., Dietrich, P., & Wollschläger, U. (2015). Estimation of catchment-scale soil moisture patterns based on terrain data and sparse TDR measurements using a fuzzy c-means clustering approach. Vadose Zone J. 14(11). doi:10.2136/vzj2015.01.0008

Seibert, J. & McGlynn, B. (2007). A new triangular multiple flow direction algorithm for computing upslope areas from gridded digital elevation models. Water Resources Research, 43, W04501. https://doi.org/10.1029/2006wr005128

Shelef, E., & Hilley, G. E. (2013). Impact of flow routing on catchment area calculations, slope estimates, and numerical simulations of landscape development. Journal of Geophysical Research: Earth Surface, 118(4), 2105–2123. doi:10.1002/jgrf.20127

Sørensen, R. & Seibert, J. (2007). Effects of DEM resolution on the calculation of topographical indices: TWI and its components. Journal of Hydrology, 347, 79-89. https://doi.org/10.1016/j.jhydrol.2007.09.001

Sørensen, R., Zinko, U. & Seibert, J. (2006). On the calculation of the topographic wetness index: evaluation of different methods based on field observations. Hydrology and Earth System Sciences, 10, 101-112. https://doi.org/10.5194/hess-10-101-2006

Tague C., Band L., Kenworthy S. & Tenebaum D. (2010) Plot- and watershed-scale soil moisture variability in a humid Piedmont watershed. Water Resources Research 46: 1–13. https://doi.org/10.1029/2009WR008078

Tarboton, D.G. (1997). A new method for the determination of flow directions and upslope areas in grid digital elevation models. Water Resources Research, 33, 309-319. https://doi.org/10.1029/96wr03137

Thomas, I. A., Jordan, P., Shine, O., Fenton, O., Mellander, P. E., Dunlop, P. & Murphy, P. N. C. (2017). Defining optimal DEM resolutions and point densities for modelling hydrologically sensitive areas in agricultural catchments dominated by microtopography. International Journal of Applied Earth Observation and Geoinformation, 54, 38-52. https://doi.org/10.1016/j.jag.2016.08.012

Wang, L. & Liu, H. (2006). An efficient method for identifying and filling surface depressions in digital elevation models for hydrologic analysis and modelling. International Journal of Geographical Information Science, 20, 193-213, http://dx.doi.org/10.1080/13658810500433453

Vaze, J., Teng, J. & Spencer, G. (2010). Impact of DEM accuracy and resolution on topographic indices. Environmental Modelling & Software, 25, 1086-1098. https://doi.org/10.1016/j.envsoft.2010.03.014

Wei, H. & Bartels, M. (2012). 3D Digital Elevation Model Generation, in: Pears, N., Yonghuai Liu, Bunting, P. (Eds.), 3D imaging, analysis and applications. New York: Springer, London, pp. xvi, 499 pages. https://doi.org/10.1007/978-1-4471-4063-4_9

Wild, J., Kopecký, M., Macek, M., Šanda, M., Jankovec, J. & Haase, T. (2019). Climate at ecologically relevant scales: A new temperature and soil moisture logger for long-term microclimate measurement. Agricultural and Forest Meteorology, 268, 40-47. https://doi.org/10.1016/j.agrformet.2018.12.018

Wilson, J. P., Aggett, G., Yongxin, D. & Lam, C. S. (2008). Water in the Landscape: A Review of Contemporary Flow Routing Algorithms, in: Zhou, Q., Lees, B., Tang, G.-a. (Eds.), Advances in Digital Terrain Analysis. Springer Berlin Heidelberg, Berlin, Heidelberg, pp. 213-236. https://doi.org/10.1007/978-3-540-77800-4_12

Wilson, J.P., (2018). Environmental Applications of Digital Terrain Modeling. Available at: http://dx.doi.org/10.1002/9781118938188

Wise, S. M. (2007). Effect of differing DEM creation methods on the results from a hydrological model. Computers & Geosciences, 33, 1351-1365. https://doi.org/10.1016/j.cageo.2007.05.003

Wolock, D. M. & Price, C. V. (1994). Effects of Digital Elevation Model Map Scale and Data Resolution on a Topography-Based Watershed Model. Water Resources Research, 30, 3041-3052. https://doi.org/10.1029/94wr01971

Wood, S. (2018). Mixed GAM Computation Vehicle with Automatic Smoothness Estimation, package 'mgcv', v. 1.8-23. https://cran.r-project.org/web/packages/mgcv/mgcv.pdf (accessed 26th April 2018).

Woodrow, K., Lindsay, J. B., & Berg, A. A. (2016). Evaluating DEM conditioning techniques, elevation source data, and grid resolution for field-scale hydrological parameter extraction. Journal of Hydrology, 540, 1022–1029. doi:10.1016/j.jhydrol.2016.07.018

Zevenbergen, L. W. & Thorne, C. R. (1987). Quantitative-Analysis of Land Surface-Topography. Earth Surface Processes and Landforms, 12, 47-56. https://doi.org/10.1002/esp.3290120107

Zhang, W. H. & Montgomery, D. R. (1994). Digital Elevation Model Grid Size, Landscape Representation, and Hydrologic Simulations. Water Resources Research, 30, 1019-1028. https://doi.org/10.1029/93wr03553

Zhou, Q. & Liu, X. (2002). Error assessment of grid-based flow routing algorithms used in hydrological models. International Journal of Geographical Information Science, 16, 819–842. https://doi.org/10.1080/13658810210149425
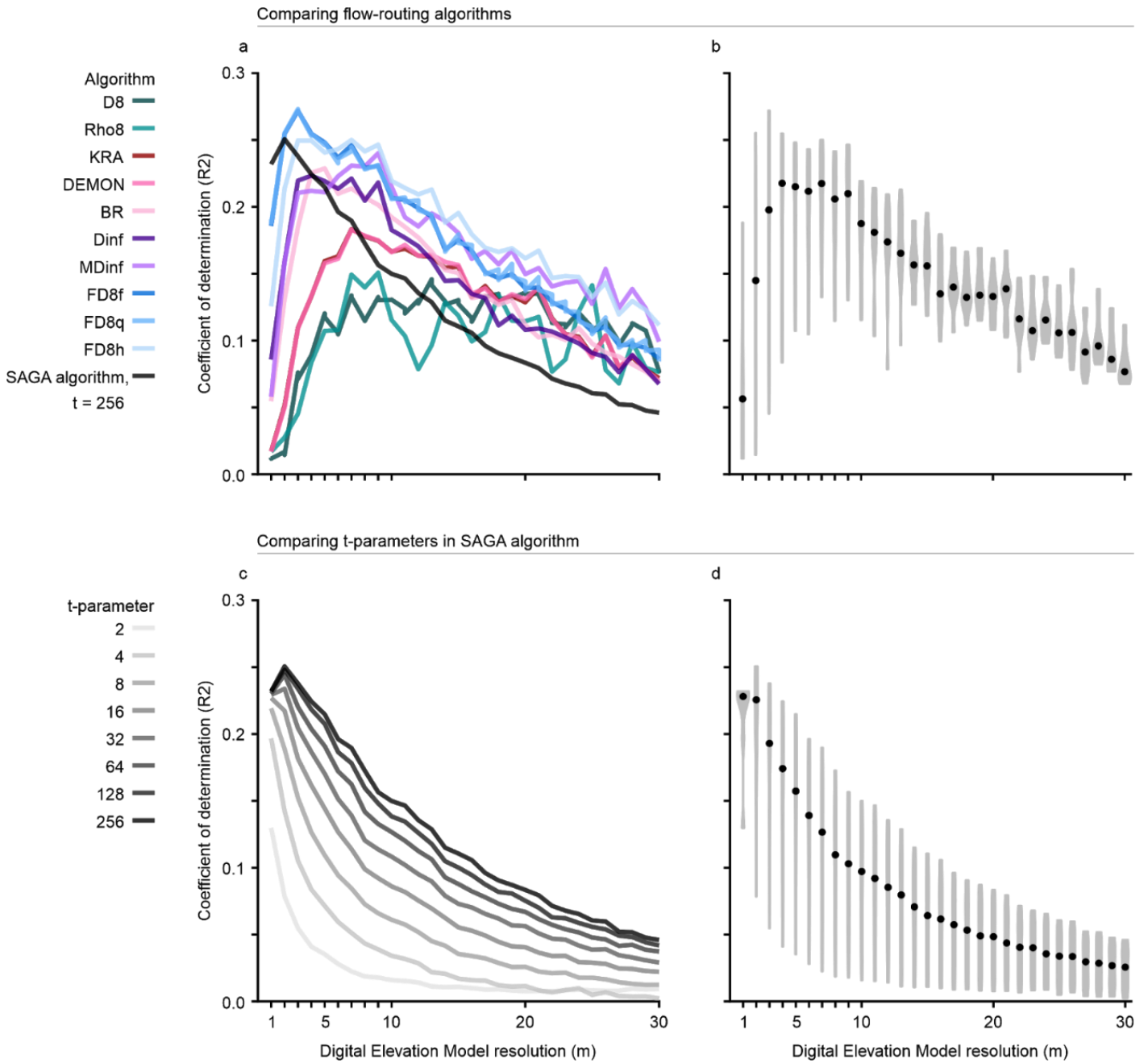
Figure S1. Comparing flow-routing algorithms and t-parameters (that is, the suction effect) with soil moisture measured at the 100 m^2-scale. (a) Lines represent the explanatory power of the flow-routing algorithms at different Digital Elevation Model (DEM) resolutions. (b) Violin plots represent the overall explanatory power of the flow-routing algorithms. (c) Lines represent the explanatory power of the t-parameters in SAGA algorithm at different DEM resolutions. (d) Violin plots represent the overall explanatory power of the t-parameters. In the violin plots (b, d), the thickness of the violin polygon corresponds to the local density of the values and the points represent the median values. Note that the y-axis expands to 0.3 (only to 0.25 in Figure 3, Figure S2, S3, S4).
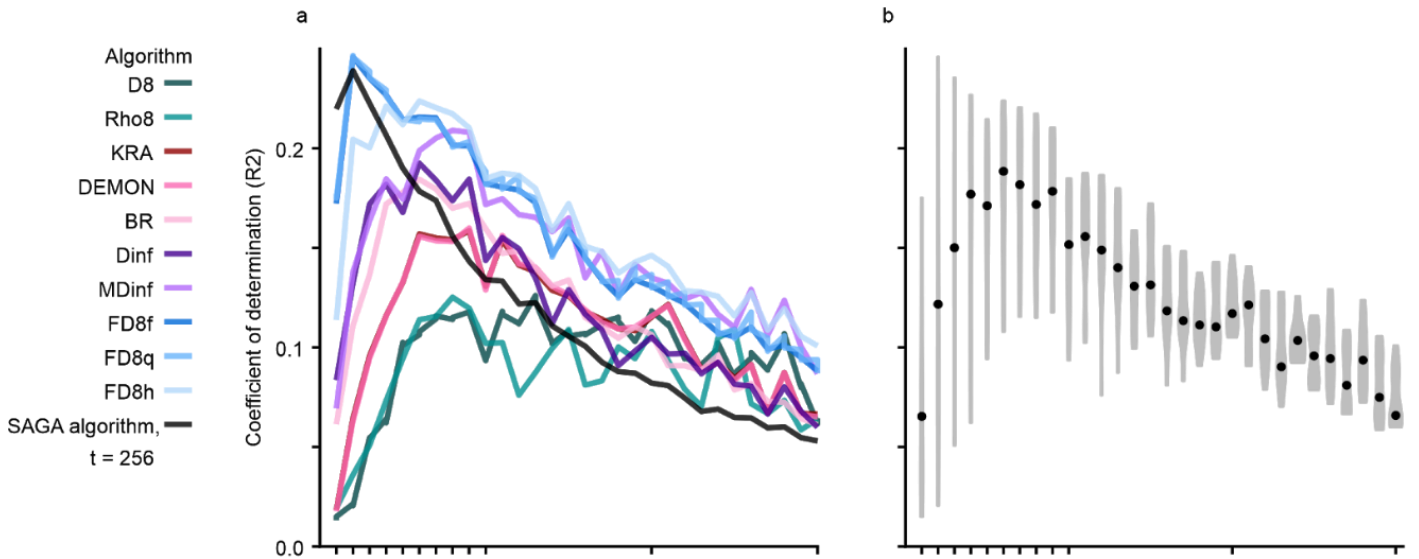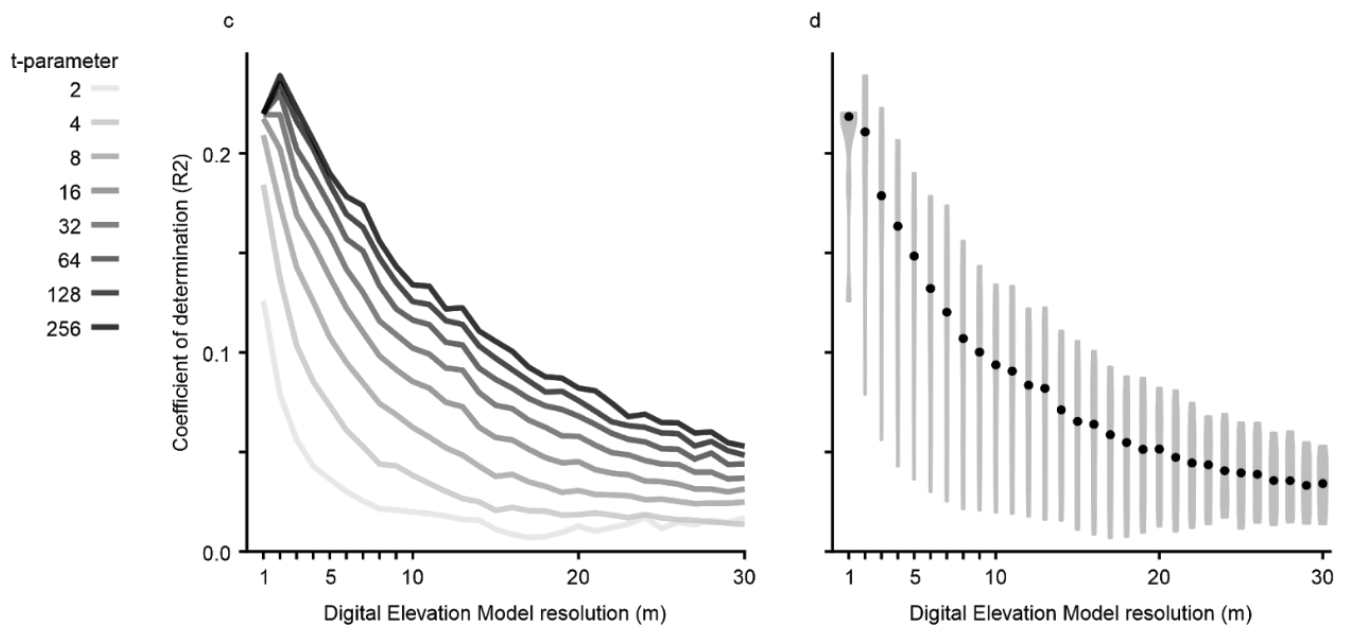
Figure S2. Comparing flow-routing algorithms and t-parameters (that is, the suction effect) with soil moisture measured in June at the 1 m²-scale. (a) Lines represent the explanatory power of the flow-routing algorithms at different Digital Elevation Model (DEM) resolutions. (b) Violin plots represent the overall explanatory power of the flow-routing algorithms. (c) Lines represent the explanatory power of the t-parameters in SAGA algorithm at different DEM resolutions. (d) Violin plots represent the overall explanatory power of the t-parameters. In the violin plots (b, d), the thickness of the violin polygon corresponds to the local density of the values and the points represent the median values.
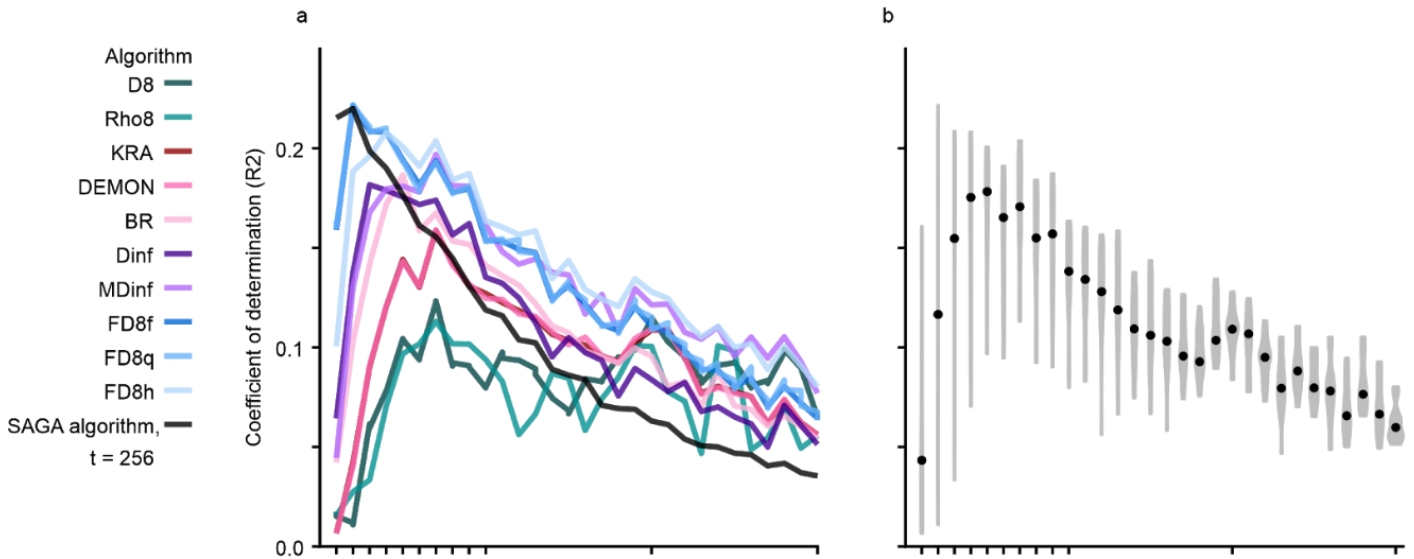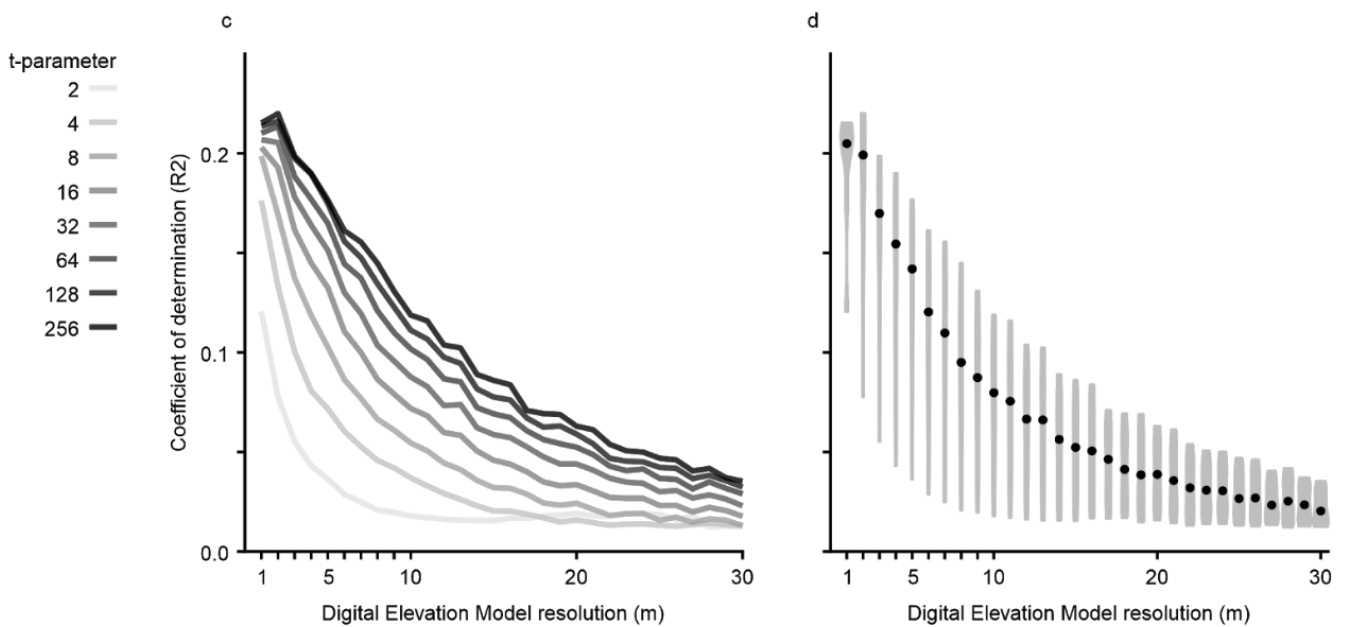
Figure S3. Comparing flow-routing algorithms and t-parameters (that is, the suction effect) with soil moisture measured in July at the 1 m²-scale. (a) Lines represent the explanatory power of the flow-routing algorithms at different Digital Elevation Model (DEM) resolutions. (b) Violin plots represent the overall explanatory power of the flow-routing algorithms. (c) Lines represent the explanatory power of the t-parameters in SAGA algorithm at different DEM resolutions. (d) Violin plots represent the overall explanatory power of the t-parameters. In the violin plots (b, d), the thickness of the violin polygon corresponds to the local density of the values and the points represent the median values.
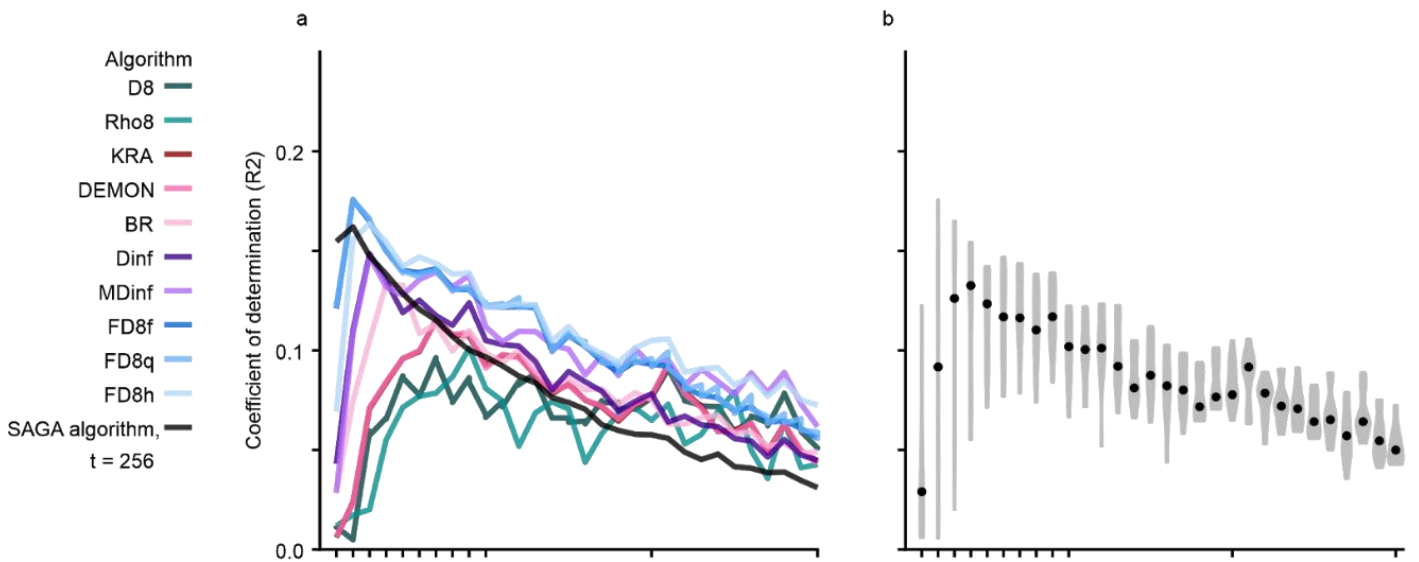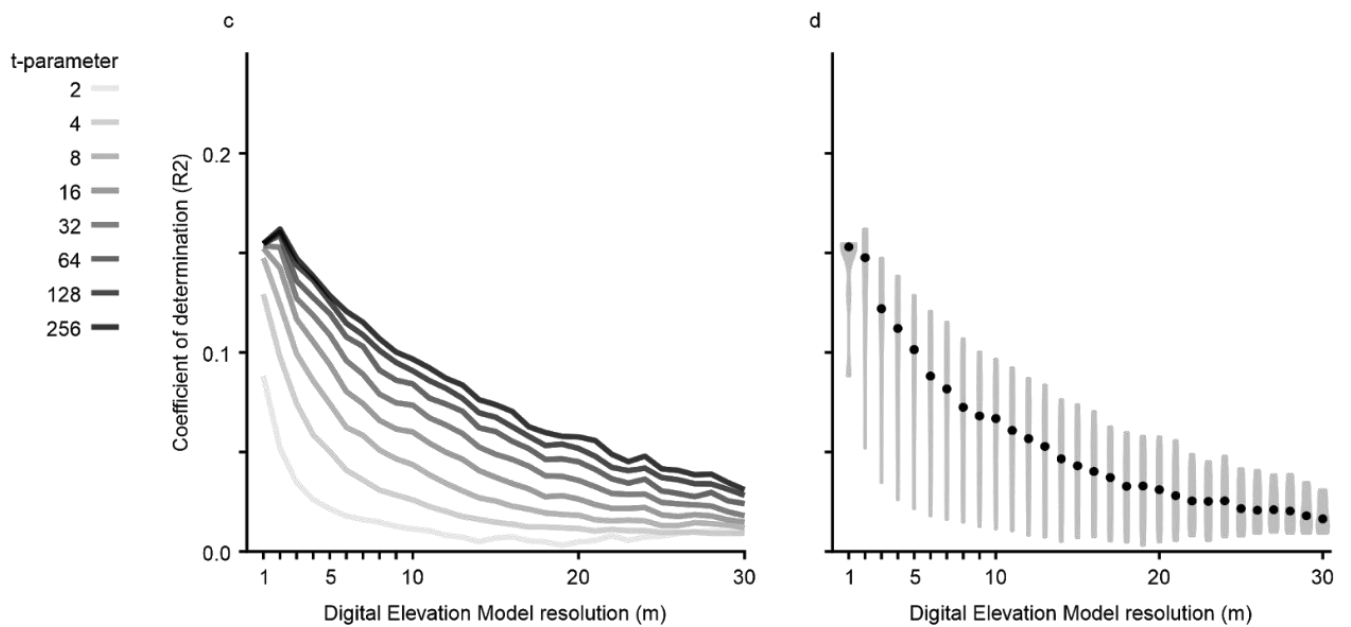
Figure S4. Comparing flow-routing algorithms and t-parameters (that is, the suction effect) with soil moisture measured in August at the 1 m^2-scale. (a) Lines represent the explanatory power of the flow-routing algorithms at different Digital Elevation Model (DEM) resolutions. (b) Violin plots represent the overall explanatory power of the flow-routing algorithms. (c) Lines represent the explanatory power of the t-parameters in SAGA algorithm at different DEM resolutions. (d) Violin plots represent the overall explanatory power of the t-parameters. In the violin plots (b, d), the thickness of the violin polygon corresponds to the local density of the values and the points represent the median values.